



Constraining Cold Nuclear Matter Effects on J/ψ production in Au+Au Collisions

D. McGlinchey¹, A. D. Frawley¹, R. Vogt^{2,3}

¹ Department of Physics, Florida State University, Tallahassee, FL 32306, USA

² Lawrence Livermore National Laboratory, Livermore, CA 94550, USA

³ University of California, Davis, CA 95616, USA

Abstract:

Recent results from PHENIX [1] on J/ψ production in d+Au collisions have shown that J/ψ's are strongly suppressed at forward rapidity. This has interesting implications for J/ψ suppression in Au+Au collisions, and may be the answer to the J/ψ puzzle. We try to constrain these cold nuclear matter (CNM) effects by fitting a parametrization of EPS09 plus a break-up cross section to the PHENIX data independently for each rapidity range. It was shown in [1] and [2] that the PHENIX R_{dAu} data at forward rapidity is inconsistent with modifications which are linearly dependent on the density-weighted longitudinal thickness of the nucleus. Therefore, in the present work, a stronger than linear dependence of the shadowing on the nuclear thickness is employed to fit the d+Au data. We find that the fitted shadowing power is large wherever the shadowing is strongest. Using this parametrization we then predict the p_T dependence of the J/ψ modification in d+Au collisions and compare with new PHENIX preliminary results. We find that at midrapidity the J/ψ R_{dAu} vs p_T is well described by the fitted shadowing plus nuclear breakup parametrization.

Introduction:

J/ψ suppression in heavy ion collisions has long been predicted to be a signature of the transition from normal nuclear matter to a quark gluon plasma (QGP). Measurements of J/ψ production in Au+Au collisions at $\sqrt{s}=200$ GeV by PHENIX [3] at RHIC show large suppression at midrapidity for central collisions, and even greater suppression at forward rapidity. This is counter to normal energy density arguments, which predict greater suppression at midrapidity. Recent PHENIX results of J/ψ production in d+Au collisions [1] show significant suppression at forward and midrapidities for central collisions. This shows that understanding the cold nuclear matter (CNM) effects is a prerequisite for interpreting the Au+Au results.

Here we attempt to constrain these CNM effects by fitting the recent PHENIX d+Au data with a parametrization that uses EPS09 shadowing plus a breakup cross section. Using this parametrization will then allow us to predict the CNM effects on J/ψ production in Au+Au collisions.

Model of the Nuclear Modification:

The nuclear modification was modeled using two components, EPS09 shadowing and a breakup cross section, with two free parameters. The first is the power of the thickness dependence of the shadowing, and the second the breakup cross section.

The modification of the J/ψ production probability was calculated on an event by event basis with a Glauber model of the nuclear collision. In each nucleon-nucleon collision the modification was calculated based on r_T , the radial position of the struck nucleon in the Au nucleus. The longitudinal nuclear thickness at the struck nucleon, $\Lambda(r_T)$, is then given by

$$\Lambda(r_T) = \int dz \rho(z, r_T), \quad (1)$$

Where A is the mass of the Au nucleus, and ρ follows, on average, a Woods-Saxon distribution with

$$\rho(z, r_T) = \frac{\rho_0}{1 + e^{\sqrt{z^2 + r_T^2} - r_{WS}}} / d_{WS} \quad (2)$$

$$\rho_0 = A \left(\frac{4}{3} \pi r_{WS}^3 \right)^{-1}, \quad (3)$$

where, as in the Glauber model, $r_{WS} = 6.38$ fm and $d_{WS} = 0.54$ fm.

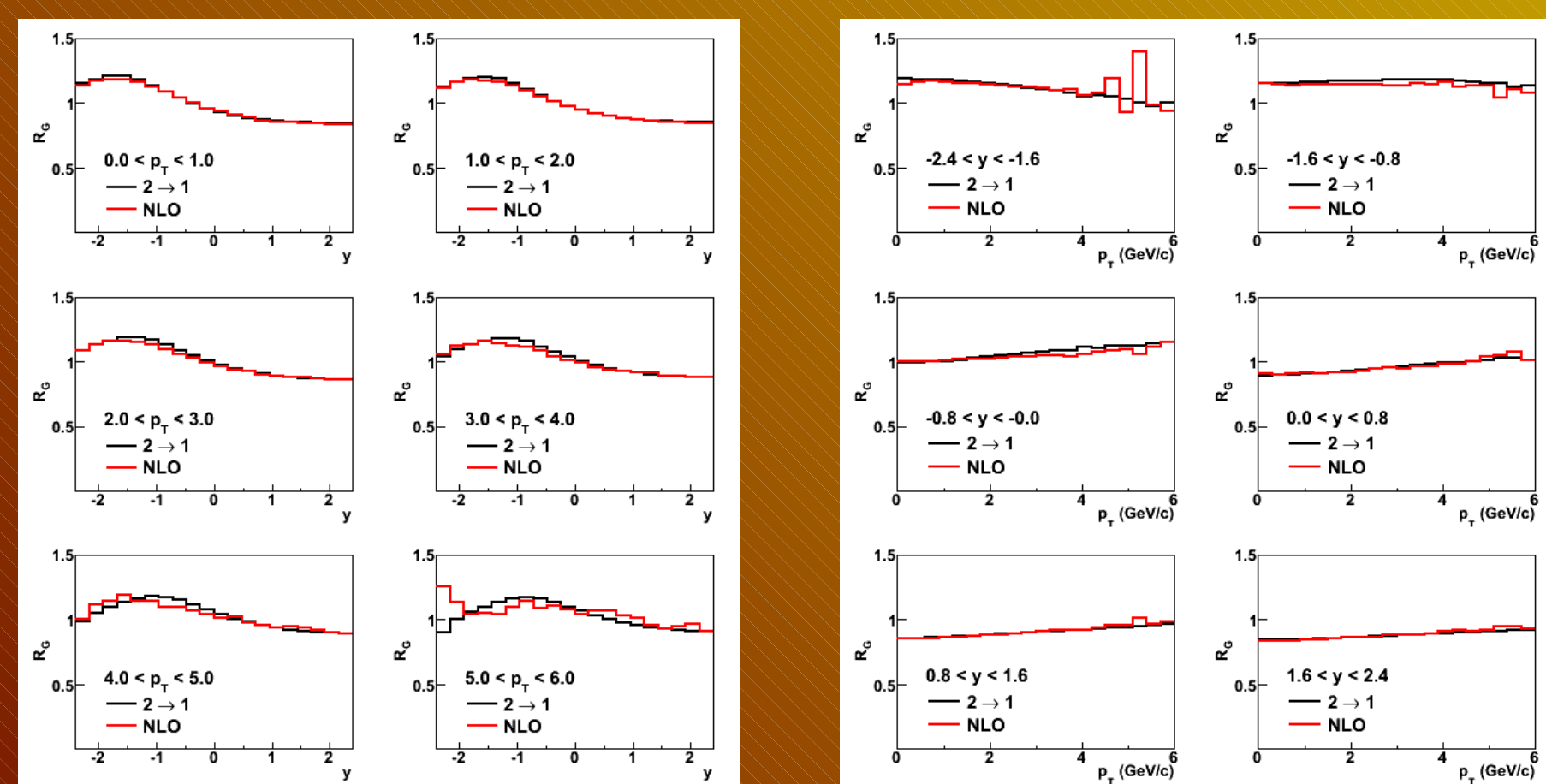


Figure 1: Comparison of EPS09 shadowing calculated with x and Q^2 taken from 100k 2→2 events calculated in NLO, and the simple 2→1 formula described below. (Left) EPS09 shadowing vs y for 6 p_T bins. (Right) EPS09 shadowing vs p_T for 6 y bins.

For each NN collision the modification from J/ψ breakup is calculated with

$$S_{br}(r_T, z_1) = e^{-\sigma_{br} \Lambda(r_T, z_1)}, \quad (4)$$

where z_1 is the z position of the struck nucleon in the Au nucleus, and σ_{br} has units of fm² and is assumed to be constant with p_T .

For each NN collision the modification due to shadowing is calculated with

$$S_{shad}(r_T, p_T, y) = 1 - \left(\frac{1 - \text{EPS09}(x, Q^2)}{a(n)} \right) \Lambda(r_T)^n, \quad (5)$$

Where the shadowing power n is an integer that is allowed to vary between 1-20. The normalization factor for a given n , $a(n)$, has units of fm² and is adjusted such that the modification for a given x and Q^2 , when integrated over all collisions, matches the EPS09 modification for the same x and Q^2 . Here x and Q^2 are calculated assuming a 2→1 process using

$$x = \frac{\sqrt{M_{J/\psi}^2 + p_T^2}}{\sqrt{s}} e^{-y} \quad (6)$$

$$Q^2 = M_{J/\psi}^2 + p_T^2. \quad (7)$$

J/ψ production via a 2→1 process is forbidden due to conservation of angular momentum, and the fact that production of a J/ψ with non-zero p_T must be accompanied by the emission of at least one balancing particle. However, a comparison between the EPS09 shadowing with x and Q^2 values from the 2→1 formulation vs a more rigorous NLO calculation based on 2→2 kinematics is shown in Fig. 1, and shows that the 2→1 process yields similar results.

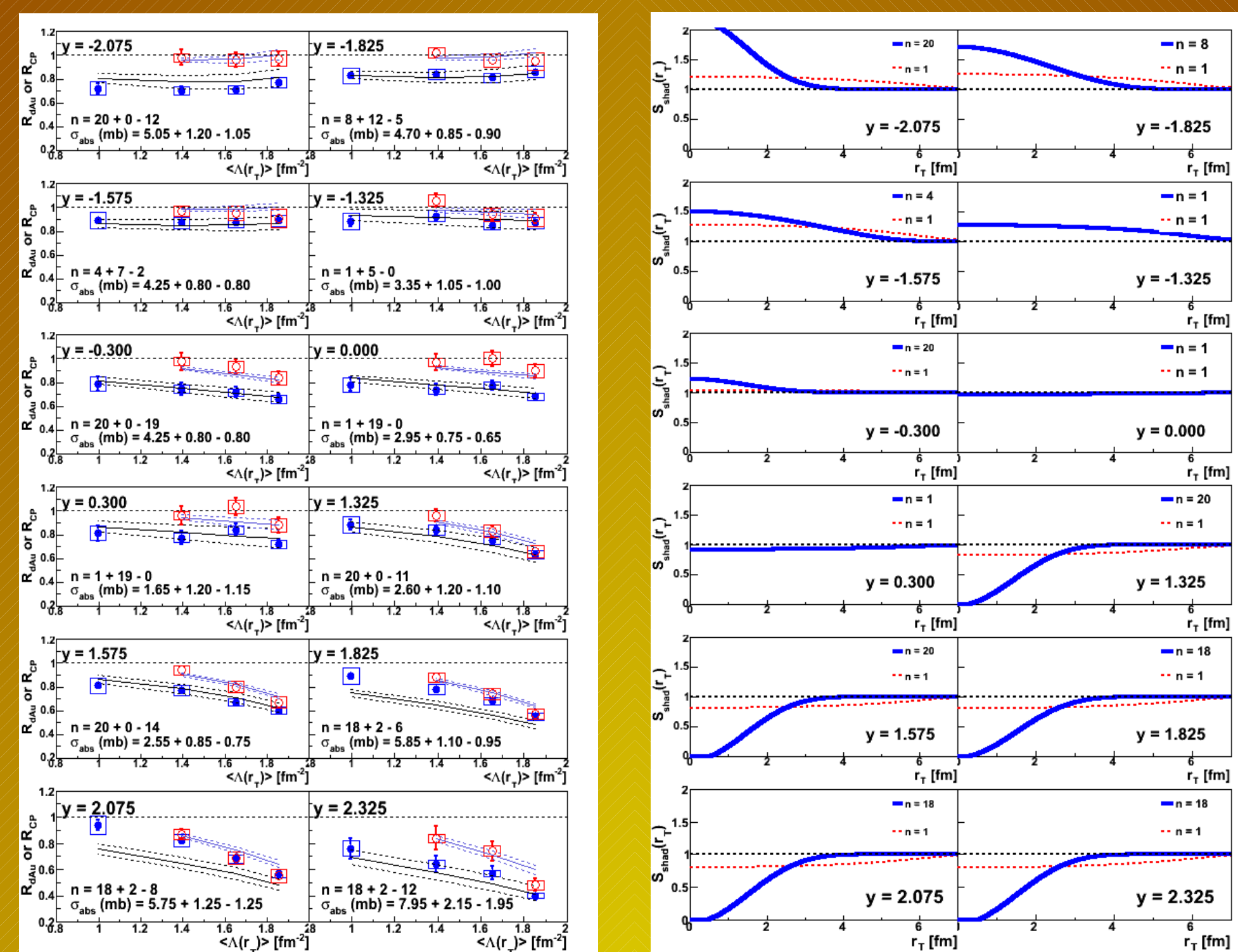


Figure 2: (Left) Fits of EPS09 NLO shadowing + break-up cross section to PHENIX R_{dAu} data [1] (blue points) vs nuclear thickness for each rapidity bin. Also shown are the PHENIX R_{CP} (red points) and the corresponding predictions from the best fit (blue lines). (Right) The nuclear modification from EPS09 vs r_T with the best fit n values. Also shown is the modification with a linear $\Lambda(r_T)$ dependence for reference.

Fitting the d+Au Data:

Using the above prescription, the total modification is calculated in the 12 rapidity intervals where the PHENIX data were measured for a series of σ_{br} (-5→15 mb in steps of 0.05) and n (1→20 in steps of 1) in a Glauber model of d+Au collisions. The Glauber model is coupled to a simulation of the PHENIX BBC trigger response to incorporate trigger efficiencies for low multiplicity events and allow for a centrality definition which matches that used by PHENIX. The rapidity and p_T values used to calculate the x and Q^2 for each NN collision are randomly sampled from distributions fitted to the PHENIX p+p J/ψ data [4].

The PHENIX J/ψ R_{dAu} data [1] was used to determine the optimum σ_{br} and n values at each rapidity using a modified χ^2 method which takes into account both the statistical and systematic uncertainties on the data points, following [5]. PHENIX reports three types of uncertainties on their data. Type A uncertainties are point-to-point uncorrelated uncertainties, dominated by statistical errors, and are represented on plots by vertical error bars. Type B uncertainties are point-to-point correlated and are represented by boxes around each data point. Type C uncertainties are globally correlated and apply to all data points, and are included as text in the figures. The modified χ^2 is defined as

$$\chi^2 = \left(\sum_{i=1}^N \frac{[R_{dAu,i} + \epsilon_B \sigma_{br,i} + \epsilon_C \sigma_{C,i} - \mu_i(n, \sigma_{br})]^2}{\sigma_{A,i}^2} + \epsilon_B^2 + \epsilon_C^2 + \epsilon_C^2 \right) \quad (8)$$

$$\tilde{\sigma}_{A,i} = \sigma_{A,i} \left(\frac{y_i + \epsilon_B \sigma_{B,i} + \epsilon_C \sigma_{C,i}}{y_i} \right) \quad (9)$$

$$\epsilon_B = \epsilon_B + 0.0646 \epsilon_s \left(\frac{\Lambda(r_T)_i}{\langle \Lambda(r_T) \rangle} - \frac{\langle \Lambda(r_T) \rangle}{\langle \Lambda(r_T) \rangle} \right) \quad (10)$$

where i is the index of the centrality bin, $R_{dAu,i}$ is the data point, $\sigma_{A,i(B,C)}$ are the type A(B,C) uncertainties on the data point, $\mu_i(n, \sigma_{br})$ is the model calculation for the given n and σ_{br} , $\epsilon_{B(C)}$ is the fraction of one standard deviation by which the data points move, and ϵ_s represents the amount by which the type B uncertainties are correlated with $\Lambda(r_T)$. The best fit values are taken to be those which produce the minimum χ^2 . The uncertainty in the value of σ_{br} was taken from the value where the minimum χ^2 was increased by 1, using the best fit shadowing power. The uncertainty in the shadowing power was taken from the value of n where the minimum χ^2 was larger than that for the best fit value of n by 1. The results of the fits to all 12 rapidity bins are shown in Fig. 2, and the best fit values are plotted vs y in Fig. 3 for convenience.

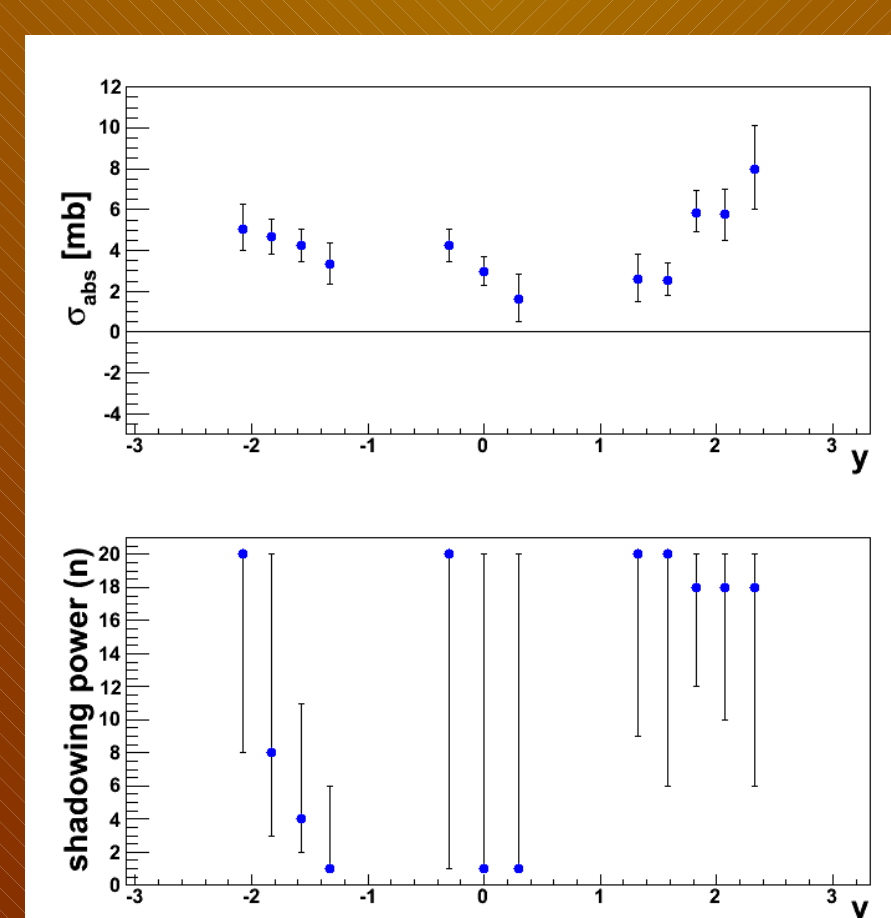


Figure 3: Best fit shadowing power (n) and σ_{br} values from Fig. 2 vs rapidity with corresponding fit errors.

References:

- [1] A. Adare et al. (PHENIX collaboration) arXiv:1010.1246
- [2] J.L. Nagle, A.D. Frawley, L.A. Linden Levy, M.G. Wysocki arXiv:1011.4534
- [3] A. Adare et al. (PHENIX collaboration) Phys. Rev. Lett. **98**, 232301 (2007).
- [4] A. Adare et al. (PHENIX collaboration) arXiv:1105.1966
- [5] A. Adare et al. (PHENIX collaboration) Phys. Rev. **C77**, 064907 (2008).

The results in Fig. 2 & 3 show two striking features. The σ_{br} values seem to have little dependence on y , although there is a suggestion that there might be a minimum at midrapidity with increases at forward and backward rapidities. The most striking feature, however, is the behavior of the shadowing power n with y . Virtually all rapidities prefer, or are consistent with, a large shadowing power. The right panel of Fig. 2 shows the EPS09 modification vs r_T for the best fit n values for each rapidity bin, as well as $n=1$ for reference. This shows that where the shadowing (or anti-shadowing) is strong, a high power is preferred, while at midrapidity, where the shadowing is weak, there is no strong preference.

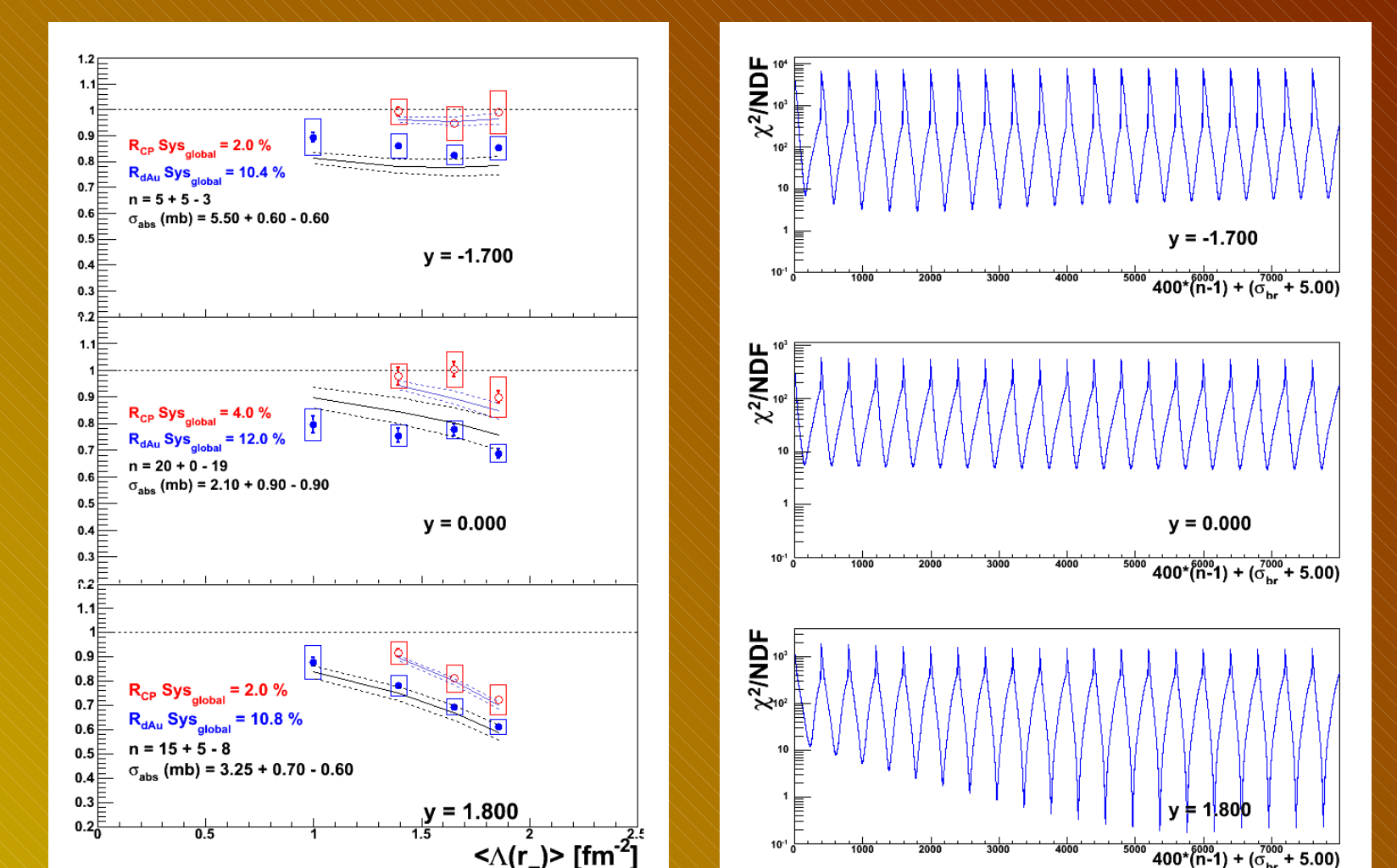


Figure 4: (Left) The PHENIX R_{dAu} and R_{CP} data integrated over the rapidity acceptance of each arm. The solid lines represent the best fit σ_{br} and n values, and the dashed curves the uncertainty band for σ_{br} . (Right) The likelihood distributions for the n and σ_{br} values. Each dip represents a different n value (1-20 from left to right) and shows the evolution of the minimum with respect to shadowing power for each rapidity bin.

We have also integrated the R_{dAu} values over the acceptance of each of the three arms. This gives the average modification across the rapidity range of the arm, and is necessary for comparing with Au+Au results. Fits to the arm integrated R_{dAu} are shown in Fig. 4 along with the likelihood distributions. The fit results are consistent with those for the 12 rapidity bin case, shown in Fig. 2.

Using the best fit σ_{br} and n values from Fig. 4, we can predict the p_T dependence of the modification due to shadowing plus breakup. This is a pure prediction, as no p_T dependence of the d+Au data is introduced into the fits. The predictions for the modification vs p_T for each arm are shown in Fig. 5 along with the new PHENIX preliminary R_{dAu} data at midrapidity. The midrapidity R_{dAu} prediction shows good agreement with the data, indicating that the EPS09 plus breakup cross section parametrization accounts reasonably well for the momentum dependence of the modification. There does not seem to be much need for physical effects (such as the Cronin effect for example) that are not included in the parametrization. It remains to be seen if this is true also at forward and backward rapidity.

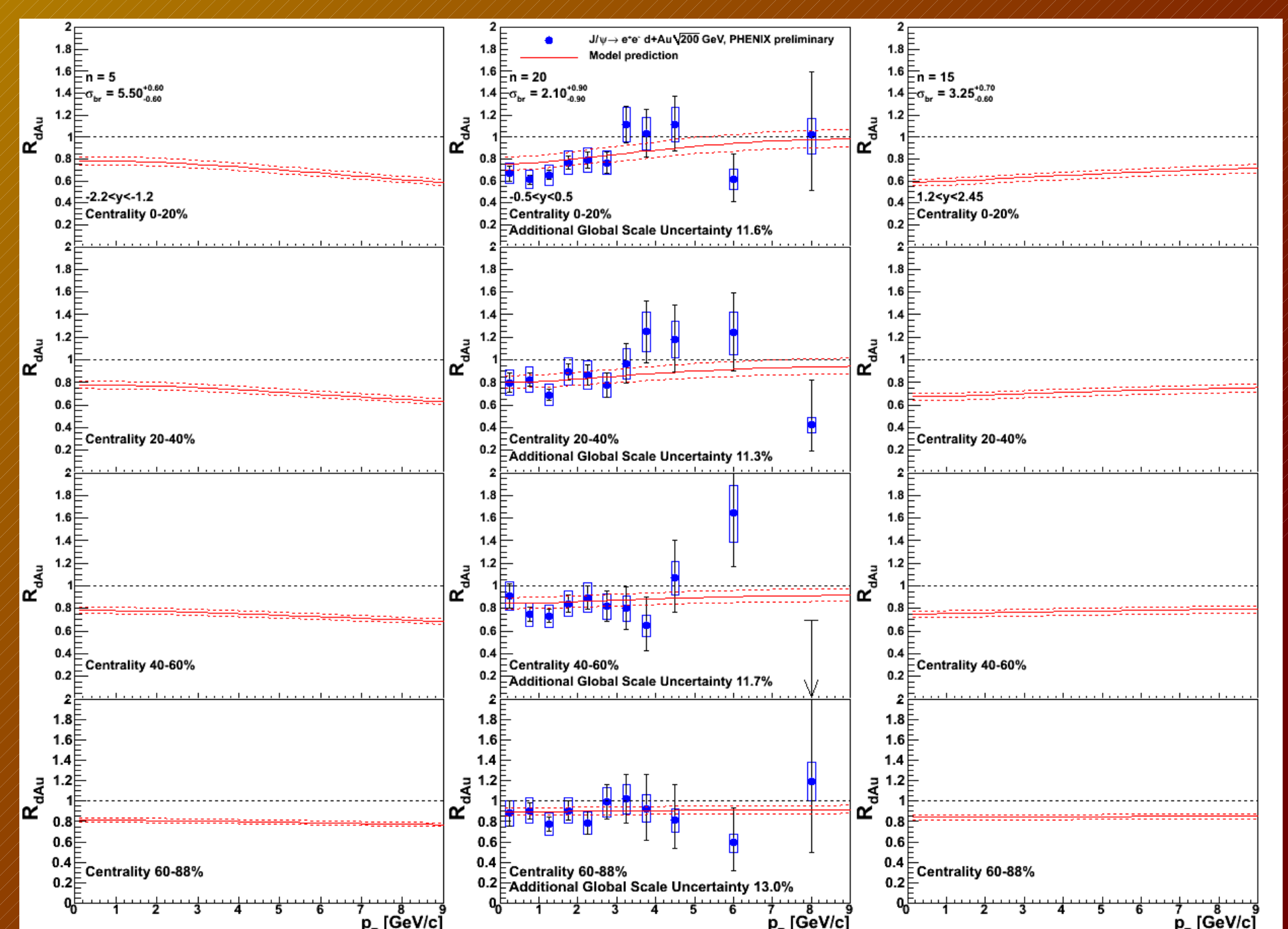


Figure 5: Predictions of the J/ψ p_T modification at each centrality from the best fit σ_{br} and n values from Fig. 4 where the solid line corresponds to the central value and the dashed lines to the uncertainty band on σ_{br} . Also shown are the midrapidity PHENIX preliminary R_{dAu} values.

Further Work:

Using the parametrization detailed here, and a Glauber model of Au+Au events, the J/ψ modification due to CNM effects in Au+Au collisions can be predicted. These effects can then be factored out of the J/ψ R_{AA} leaving only the effects due to the produced medium.

The work of D. McGlinchey and A.D. Frawley is supported by the National Science Foundation Grant NSF PHY-0754674. The work of R. Vogt was performed under the auspices of the U.S. Department of Energy by Lawrence Livermore National Laboratory under Contract DE-AC52-07NA27344 and was also supported in part by the National Science Foundation Grant NSF PHY-0555660.